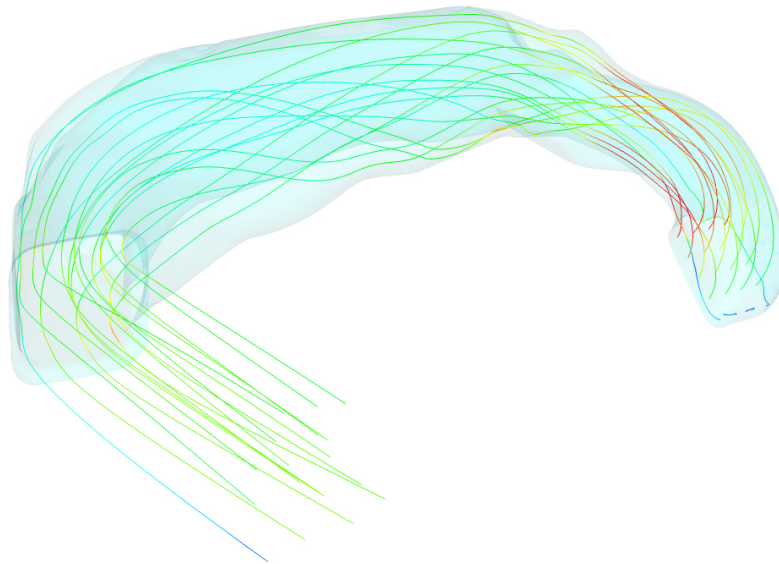# CHALMERS

Duct optimization using CFD software 'ANSYS Fluent Adjoint Solver'.

Master's thesis in Automotive Engineering

ATHANASIOS TZANAKIS

Department of Applied Mechanics

Division of Vehicle Engineering and Autonomous Systems

CHALMERS UNIVERSITY OF TECHNOLOGY

Göteborg, Sweden 2014

Master's thesis 2014:43

MASTER'S THESIS IN AUTOMOTIVE ENGINEERING

Duct optimization using CFD software 'ANSYS Fluent Adjoint Solver'.

ATHANASIOS TZANAKIS

Department of Applied Mechanics
Division of Vehicle Engineering and Autonomous Systems
CHALMERS UNIVERSITY OF TECHNOLOGY

Göteborg, Sweden 2014

Duct optimization using CFD software 'ANSYS Fluent Adjoint Solver'.
ATHANASIOS TZANAKIS

Cover:
Initial and optimized ventilation duct.

Duct optimization using CFD software 'ANSYS Fluent Adjoint Solver'.
Master's thesis in Automotive Engineering
ATHANASIOS TZANAKIS
Department of Applied Mechanics
Division of Vehicle Engineering and Autonomous Systems
Chalmers University of Technology

Abstract

The ordinary duct development procedure in Climate sector at VVC relies on the manual evaluation of the CFD results and the identification of the proper geometry changes in order to optimize the ducts shape. A newly introduced methodology in automotive sector, the adjoint procedure, could reduce the duration of a duct development process through an automatic iterative procedure. Having computed the flow results, the adjoint obtains the geometry's sensitivity field which depicts the potential changes in the domain with respect to the cost function. Then a morphing tool utilizes that data and properly modifies the geometry. The current thesis is focused on experiencing and demonstrating the merits of the adjoint solver aiming to minimize the cost function, the pressure drop, over a duct domain.

The discrete adjoint method was applied to different geometries from the Climate sector examining the prerequisites for extended adjoint use. Through those geometries both the adjoint solver and the morphing tool limitations were discovered. The limitations are mostly related to the mesh, the adjoint discretization scheme as well as the boundary constraints. During the thesis, the limitations were identified and properly examined, proposing solutions. An adequate adjoint solution was obtained when using a coarse Polyhedral mesh with cell skewness around 0.8, a low discretization scheme and a simplified geometry. Even if some compromises were required in whole procedure, the adjoint has managed to handle all the given geometries. Moreover, new optimized domains with respect to the cost function, the pressure drop minimization, were developed.

The result of the thesis was a guide of how to overcome adjoint constraints as well as an analytical illustration of the adjoint results. In some cases, the pressure drop was minimized by 60% resulting in a smooth pressure distribution over the given domain. However, a compromise in the morphing tool leaves room for improvement on the suggested methodology.

Acknowledgements

Contents

1   Introduction

Finding the optimum solution in a given flow domain relies on both accurate flow prediction through Computational Fluid Dynamics (CFD) simulations and also on design methods, appropriate to generate new optimum configurations.

Many optimization methods already exist, yet their limitations with respect to required time as well as their efficiency of handling many design variables, define the proper method for each case. The gradient based method is the most well known method that can cope with many design variables. The gradient of the cost function is the key factor for the further shape optimization [9].

Numerical optimization methods in combination with flow simulations could be used to face the design problem.These methods require the gradient of the objective function with respect to modifications in the desirable variable in order to define the magnitude of domain change. Finite difference method is the simplest way to calculate those gradients. However, it requires an iterative procedure as the gradient components are obtained by independently changing each design variable with finite step ,calculating the desired objective function using CFD analysis and estimating the ratio of differences. In each iteration the local minimum or maximum of the objective function is calculated and the process is repeated until the gradient tends to zero [9]. So, in case of perturbing N points on the given surface, N flow simulations are required to obtain the data set which lead to optimum solution [2] .

Consequently,the finite difference method requires high computational time as the design variables N are increasing. In contrast, adjoint method is able to obtain design sensitivities of a function with respect to many design variables in a single adjoint computation. This implies that the computational cost for the gradient calculation is equal to that for solving the flow equations. The adjoint is implemented into a finite volume solver using either continuous or discrete approach [2]. In the current study, ANSYS FLUENT applies the discrete approach due to its ability to provide more robust sensitivity information in cases with complex geometry configurations [2].A converged adjoint solution provides the domain morphing sensitivities, identifying the areas where the domain mesh should be modified.The ANSYS FLUENT mesh adaption method is based on gradient algorithm , adjusting the system in a way that maximizes the effect of change. For instance, in areas where sensitivity is relatively high, small modification in shape will lead to high impact on the objective function. Additionally, a smooth and equally distributed deformation is applied on the surface with respect to the cost function[2].

The adjoint method has been used as an optimization tool in the aerodynamics field since 1984. Adjoint solver has been introduced by Pironneau and firstly applied to shape design for Elliptic Systems [8] .In the current study, adjoint method is focused on internal flows and having as objective function the pressure drop minimization. For that purpose, a variety of parameters which could influence both the adjoint solution and the morphing feature have been investigated. The mesh type and skewness as well as the adjoint discretization scheme are few of the parameters that sticks out as important factors for establishing a robust methodology. Moreover, the results of four different cases which illustrate different topology limitations as well as morphing constraints,are presented in the report .

Firstly, a geometry of a front floor duct was given which was analyzed in scope of compatible mesh generator with adjoint solver in terms of mesh quality. In that case, the entire geometry was morphed without limitations aiming to obtain an overall knowledge around both adjoint and morphing tool. Later on, rear floor duct was examined, where issues related with type of mesh and morphing feature were observed. Once all issues were addressed, adjoint methodology was applied in more complex and demanding geometries of B-pillar duct and front ventilation system. However, some new adjoint constraints came up ,yet they were worked out through compromises in morphed areas.

1.1 Purpose

The current study will evaluate the possibilities for VCC to use 'ANSYS Fluent Adjoint Solver' when developing ducts to the car ventilation system. This involves investigating prerequisites and restrictions with the software as well as robustness and ease of use. The main delivery from the thesis will be a verdict on the possibility of using the Adjoint Solver for a duct optimization and also a best practice guideline of how to use it.

1.2 Background

The shape of a duct in a car climate system is rarely designed from a fluid dynamic point of view. The competition of space is intense when developing a new car and the ducts are often squeezed in between other components. As a result, the duct shape can be very complex and finding optimal shape improvements is not intuitive. In order to speed up the development process of an air ventilation duct and also find the best possible solution in terms of fluid dynamic performance, we are interested in evaluating 'ANSYS Fluent Adjoint Solver'. After a CFD solution is computed, 'ANSYS Fluent Adjoint Solver' identifies which regions of a shape are most sensitive to changes with respect to a defined quantity of interest. That data can then be used as input for morphing of the volume or surface mesh and the shape can be optimized in terms of the quantity of interest.

2 Theory

In the current chapter the flow field governing equations and their discretized form, are presented. Moreover, the gradient based optimization methods as well as the advantages of adjoint approach, are briefly discussed. As the discrete adjoint approach is applied in that study, a further analysis of this approach takes place. At the end of the chapter the basic theory of ANSYS mesh morphing method is presented. This method is applied after obtaining the surface sensitivity field through the adjoint solver.

2.1 The governing equations

The numerical analysis of the current duct flow study relies on assumption of incompressible and isothermal flow. The incompressible continuity equation is described by,

$$\frac{\partial u_i}{\partial x_i} = 0 \tag{2.1}$$

since the flow field is described by Newtonian fluid the Navier - Stokes equations can be written in the following form for the development of the finite volume method,

$$\rho \frac{\partial u_i}{\partial t} + \rho u_j \frac{\partial u_i}{\partial x_j} = -\frac{\partial p}{\partial x_i} + \frac{\partial \overline{\tau}_{ij}}{\partial x_j} \tag{2.2}$$

where $\overline{\tau}_{ij}$ represents the viscous stress components.

$$\overline{\tau}_{ij} = \mu \left(\frac{\partial u_i}{\partial x_j} + \frac{\partial u_j}{\partial x_i} \right) \tag{2.3}$$

The turbulent flow calculation was numerically analyzed by Reynolds-averaged Navier-Stokes equations. This method is focused on the mean flow, obtaining a time averaged solution to the Navier Stokes equation. In order to achieve that, the instantaneous part $\varphi_i(x, t)$ is divided into mean,$\Phi_i(x)$ and fluctuating $\varphi_i'(x, t)$. The Reynolds decomposition is applied into instantaneous velocity and pressure, respectively.

$$u_i(x, t) = U_i(x) + u_i'(x, t) \tag{2.4}$$

$$p_i(x, t) = P_i(x) + p_i'(x, t) \tag{2.5}$$

Inserting equation 2.4 and 2.5 into 2.2, as well as considering the time average of the fluctuation to be zero $\varphi_i'(x, t)$,the following equation is obtained,

$$\frac{\partial U_i}{\partial x_i} = 0 \tag{2.6}$$

$$\rho \frac{\partial U_i}{\partial t} + \rho U_j \frac{\partial U_i}{\partial x_j} = -\frac{\partial P}{\partial x_i} + \frac{\partial \overline{\tau}_{ij}}{\partial x_j} \tag{2.7}$$

where total stress $\overline{\tau_{ij}}$ is now the sum of the viscous and the turbulent stress,

$$\overline{\tau}_{ij} = \mu \left(\frac{\partial U_i}{\partial x_j} - \rho \overline{u_i' u_j'} \right) \tag{2.8}$$

Introducing the *Bousinesq* assumption, the turbulent viscosity μ_t , which is flow dependant in contrast to laminar μ, is added. So, the total stress is now formed as,

$$\overline{\tau}_{ij} = \mu_t \left(\frac{\partial U_i}{\partial x_j} + \frac{\partial U_j}{\partial x_i} \right) - \frac{2}{3} \rho k \delta_i j \tag{2.9}$$

3

2.2 Wall function

A boundary layer is created while a fluid is flowing along a body surface. Near the surface the velocity is zero, and it is increaing until it reaches the free stream velocity. The turbulent layer can be divided into three parts, one laminar ,one turbulent and a mixture of both. Near the wall, flow is divided in three regions, the viscous sublayer, the buffer layer and the fully turbulent lag-law layer. Those region are illustrated in Figure 2.1, plotted with semi-log coordinates.
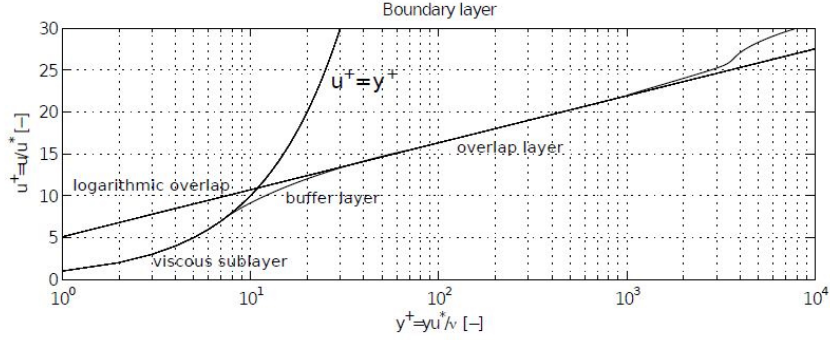

Figure 2.1: *Law of the wall* .

In the x-axis the non-dimensional wall distance is defined as,

$$y^+ = \frac{yu^*}{\nu} \tag{2.10}$$

where friction velocity is u^* ,ν is kinematic viscosity and y is the height of the first cell. The Enhanced Wall Treatment ϵ-Equation model which combines a two layer model with the so-called enhanced wall function, was used [2]. Reasonable results could be obtained in the areas with $y+ <5$ and $y+>30$ where the two layer model and the wall function perform better, respectively.

2.3 Optimization Methods

The development of shape optimization methods coupled with computational fluid dynamics has been a topic under investigation for decades. The necessity to reduce the time invested into the development cycle, from initiation until the final product release, has lead to the appearance of different optimization methodologies.

A key factor that defines the utility of an optimization method is the ability to handle many design variables such as multiple shape modifications of a given geometry. The gradient based method can cope with many design variables, computing the gradient of the cost function which is key factor for further shape optimization [9]. Since the duct optimization involved many design variables, the gradient based method has been applied in order to achieve the optimum shape with respect to the objective function,the pressure drop minimization. This method is resolved through different computational schemes such as the finite difference scheme and the adjoint approach. Adjoint approach requires less computational time to derive the gradient of the cost function than finite difference scheme, mainly due to the fact that it needs a single run to compute the gradient, being independent from design variables.

Furthermore, the adjoint method is spited into the continuous and the discrete approach. In the continuous approach the adjoint equation is analytically derived from the governing equations and get discretized afterwards. In contrast, the discrete approach, the governing equation is initially discretized and the discrete adjoint equation is computed afterwards. That difference is illustrated schematically in Figure 2.2 where the two different approaches are compared [4].

In order to compare the discrete and continuous approach , the user preferences as well as the objective function that is going to be investigated should be taken into account. The fact that it uses the same solvers as those for transport equations, could be considered a benefit of the discrete approach. In contrast, applying the continous approach might require different discretization schemes. Using schemes as close as those in
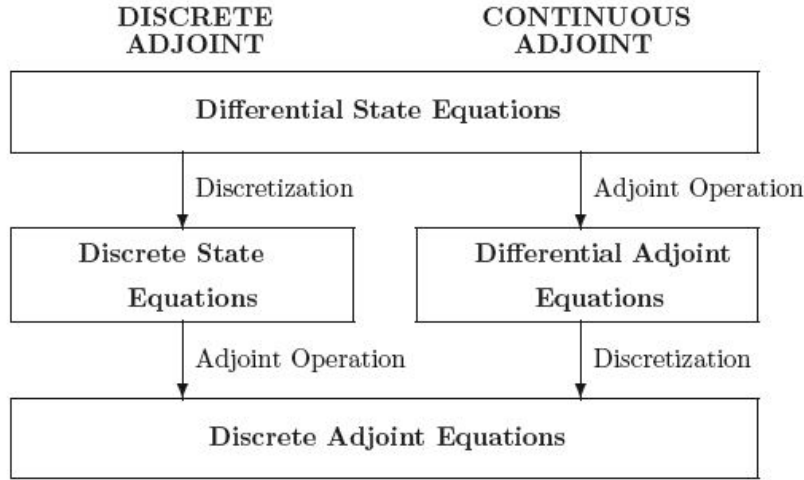
Figure 2.2: *Discrete and continuous approach [11]* .

transport equations yields to more accurate gradient computation. Moreover, the grid limitations could occur in differences in the gradient values calculated by the above approaches [11].

In the current report only the discrete approach has been used , as ANSYS FLUENT uses this approach due to its ability to provide more robust sensitivity information in cases with wall functions and complex geometry configurations [2]. The following sector will be focusing on the derivation of discrete adjoint solver providing a wider view of that method.

2.4 The discrete adjoint approach

The adjoint solver has as a prerequisite a fully converged flow simulation, from which the gradients of objective function will be derived. In our case the objective function, I, is pressure drop and is defined as

$$I = I(\overline{\omega}, \zeta) \tag{2.11}$$

where $\overline{\omega}$ and ζ represent the flow field variables and physical location of the boundary, respectively. A change in boundaries ζ results in the objective function.

$$\delta I = \frac{\partial I^T}{\partial \overline{\omega}} \delta \overline{\omega} + \frac{\partial I^T}{\partial \zeta} \delta \zeta \tag{2.12}$$

The adjoint is applied in the flow field which is depending on $\overline{\omega}$ and ζ. Thus the flow field is a constraint of the optimization problem. The governing equations is

$$R(\overline{\omega}, \zeta) = 0 \tag{2.13}$$

The optimization should operate between the defined limitations of the flow flied, such as flow and design variables. That leads to zero variation of R,

$$\delta R = 0 = [\frac{\partial R}{\partial \overline{\omega}}] \delta \overline{\omega} + [\frac{\partial R}{\partial \zeta}] \delta \zeta \tag{2.14}$$

The Lagrange Multiplier ψ is introduced aiming to convert a constrained optimization problem to unconstrained

optimization problem. So the equation *2.2*,

$$\delta I = \frac{\partial I^T}{\partial \overline{\omega}} \delta \overline{\omega} + \frac{\partial I^T}{\partial \zeta} \delta \zeta - \psi^T \{ [\frac{\partial R}{\partial \overline{\omega}}] \delta \overline{\omega} + [\frac{\partial R}{\partial \zeta}] \delta \zeta \}$$
$$= \{ \frac{\partial I^T}{\partial \overline{\omega}} - \psi^T [\frac{\partial R}{\partial \overline{\omega}}] \} + \{ \frac{\partial I^T}{\partial \zeta} - \psi^T [\frac{\partial R}{\partial \zeta}] \}$$

(2.15)

Choosing ψ to eliminate flow variations terms, an explicit expression for the derivative of the objective function with respect to the design variables only, is derived. So the adjoint equation is obtained and it should be solved.

$$[\frac{\partial R}{\partial \overline{\omega}}]^T \psi = \frac{\partial I}{\partial \overline{\omega}}$$

(2.16)

Inserting the adjoint equation to equation 2.15 an equation between cost function and design variables is derived.

$$\delta I = \{ \frac{\partial I^T}{\partial \zeta} - \psi^T [\frac{\partial R}{\partial \zeta}] \} \delta \zeta$$
$$= G^T \delta \zeta$$

(2.17)

where G represents the desired gradient of the cost function with respect to design variables ζ and the flow solution R.

$$G = \frac{\partial I^T}{\partial \zeta} - \psi^T [\frac{\partial R}{\partial \zeta}]$$

(2.18)

As it is seen, the design sensitivity vector is composed by two partial derivatives, the so called geometric and flow field sensitivity respectively. The geometric sensitivity shows how surface perturbing effects the cost function, on the other hand the flow field sensitivity term refers to the effect on the objective function due to flow field changes.

The advantage of the adjoint method in comparison with finite deference method is pointed out in equation 2.16 which is required to be solved once in order to obtain the design sensitivity vector with respect to design variables. The surface sensitivity information has been derived since the design sensitivity is solved. The surface mesh of the given geometry would be moved according to the following equation [6].

$$\delta \zeta = -\kappa G$$

(2.19)

where κ is positive and small enough in order for the first iteration to compute an estimation of δI ,as in equation 2.17. The κ factor is small due to linear approximation of the cost function caused by shape variations. That variation is computed as,

$$\delta I = -\kappa G^T G < 0$$

(2.20)

Consequently, δI is always negative and cost function will be minimized during iterative changes [6].

2.5   Mesh morphing

Having computed the sensitivity field through adjoint equation, the mesh modification takes place forming properly the volume mesh of the geometry. Yet, the sensitivity field may include non-smooth areas where shape modification is hard to be applied. Mesh morphing procedure has a double role. Firstly, it smooths the surface sensitivity field and secondly provides smooth distortion in boundary and interior mesh.

Having defined the desired boundaries that would be morphed, a rectangular volume encloses them. Around the control volume arrays of control points are set. These points in combination with the local mesh coordinates will define the proper movement both on the boundary and in the interior mesh. The local coordinate system relies on the properties of Bernstein polynomials. The standard coordinates of nodes in the mesh , $\underline{x}^k$, are defined by a local coordinate, (u^k, ν^k) [2] . Assuming that a control volume has $l \times m$ control points, the linear relationship between the kth grid node position and the ij^{th} control point location is

$$\underline{x}^k = \sum_{ij=0}^{l,m} \xi^{i,j} B_{i,l}(u_k) B_{j,m}(\nu_k) \tag{2.21}$$

where $B_{i,l}$ is the ith Bernstein polynomial of degree l,

$$B_{i,l}(u) = \binom{l}{i} u^i (1-u)^{n-i} \tag{2.22}$$

and $\xi^{i,j}$ represents the coordinate of the ij^{th} control point.

When a movement is applied on control points, the mapping generates a smooth repositioning of the grid nodes. Mapping mesh nodes as well as control points lead to,

$$\delta I = \sum_{ij=0}^{l,m} \delta \xi^{ij} \cdot \underline{\tilde{W}}^{ij} \tag{2.23}$$

where

$$\underline{\tilde{W}}^{ij} = \sum_n \frac{\partial I}{\partial \underline{x}^n} B_{i,l}(u_n) B_{j,m}(\nu_n) \tag{2.24}$$

is the control point sensitivity field and $\delta \xi^{ij}$ is the adjustment to the control point position. Usually, the number of grid nodes dominates over the number of control points so equation 2.14 works as a smoother on the sensitivity field. The boundary smooth mesh deformation is applied as the cost function gradient is obtained[2]. A more analytical form of equation 2.19 could be the following,

$$\delta \xi^{ij} = \kappa \underline{\tilde{W}}^{ij} \tag{2.25}$$

Moreover, if it is required,only specific areas of the surface could be morphed excluding others by setting constraints on the control point gradient field. So, the locked nodes, keep their initial position without getting involved in any deformation process[2]. Apparently, locking many nodes leads to less available morphing surface and consequently,no favorable change in cost function is observed.

3 Method

In the course of the current study a detailed methodology has been developed aiming to cope with the pressure drop minimization over ducts. This Chapter describes the initial steps which were considered in order to approach the adjoint solution. The general method followed and more detailed parameters, such as adjoint solution controls and stabilization schemes, are presented on the following sectors. At the end of the chapter the given geometries where adjoint was applied, are illustrated.

3.1 The general method

A general overview of the followed procedure is seen in Figure 3.1. The gradient of the cost function with respect to design variables, is computed when both a flow(Navies Stokes equations) and an adjoint simulation are fully converged. Based on the calculated sensitivity field, the morphing tool which modifies the boundary as well as the interior mesh inwards or outwards is applied. What follows, is the flow simulation of the morphed case and the loop of adjoint where the morphing tool iteratively runs until the optimum solution is obtained. Once the optimization is over, the boundary mesh is exported, wrapped and re-meshed in ANSA. This geometry is evaluated through a last flow simulation. The following Figure 3.1 illustrates the described methodology,
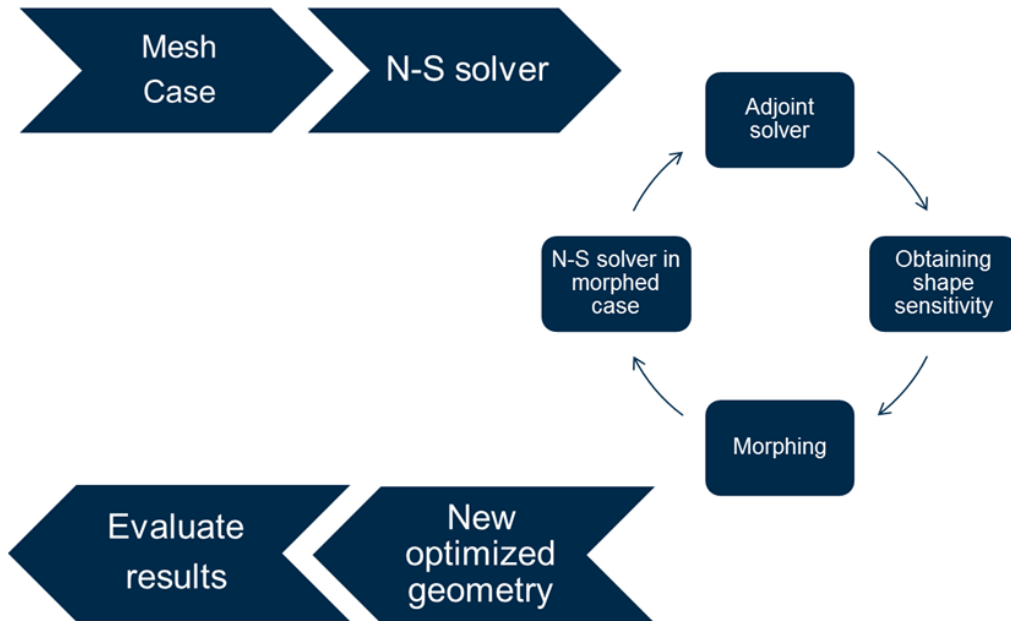

Figure 3.1: *Adjoint methodology.*

The thesis is mainly focused on setting a robust loop procedure which results in a reliable adjoint solution. It is important that an adjoint loop is fed by an adequate mesh and flow solution which effect the loop iterations. For example, bad cell quality yield either in a diverged adjoint solution or in the appearance of negative volume cells during the initial and morphing loop step, respectively. In both cases, the loop breaks without providing any significant results. Moreover, the loop robustness is effected by adjoint and morphing setting that are presented on the upcoming pages.

3.2 Setting up the simulation

The adjoint solver utilizes the flow simulation data in order to compute the surface sensitivities. Thus, a brief presentation of how the flow simulations were set up,follows.

The settings of flow simulations have been predefined and based on the Climate sector macro files since the scope of the thesis was only the adjoint solver investigation. The simulations were steady sate and isothermal. The two equations realizable k-ϵ , was set as turbulence model. The near-wall treatment was defined as the Enhanced wall Treatment which is described on Chapter2.2. The pressure and the velocity coupling was computed by coupled scheme and the Green-Gauss Cell-Based Gradient approach was preferred as the gradient discretization scheme. The momentum, turbulent kinetic energy and the turbulent dissipation rate was discretized by second order upwind scheme. The Coupled scheme required some extra settings. Thus, the flow courant number was set to 20 and the momentum and pressure explicit relaxations factors were both set to 0.4.

3.3 Adjoint solution controls

The ANSYS adjoint solver interface let the user adjust some parameters that might influence the adjoint convergence such as the advancement controls and the stabilization schemes. Starting with the advancement controls, there is the choice of either preconditioning solution or not. This is required for the most cases involving turbulent flow. As it is activated, the options of the Courant number, the Artificial compressibility and the flow rate Courant scaling are appeared having their default values. The interface of the adjoint control settings is shown in Figure 3.2
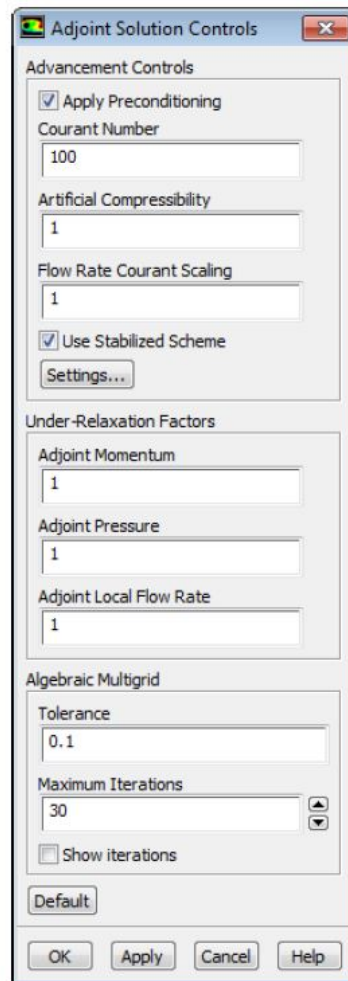

Figure 3.2: *Adjoint solution controls.*

3.3.1 Courant Number

The Courant-Fredrichs-Lewy condition is a stability requiremnet for solving PDE numerically by the method of the finite differences. For one dimensional case, the CFL is expressed as [3],

$$C = \frac{u\Delta t}{\Delta x} \leq C_{max} \tag{3.1}$$

where Δt is the time step, Δx is dimension of the grid cell at each location, u represents the average linear velocity and C_{max} varies as follows,

$$C_{max} = \begin{cases} \leq 1 & \text{if an explicit (time marching) solver is used,} \\ >1 & \text{if an implicit solver is used.} \end{cases} \tag{3.2}$$

Our solver is not time marching so higher values than one could be used.

3.3.2 The artificial compressibility method

The artificial compressibility method is an approach in order to overcome the difficulty of the pressure decoupling

$$\frac{\partial p}{\partial t}\frac{1}{\beta} + \frac{\partial u_i}{\partial x_i} = 0 \tag{3.3}$$

where β is the artificial compressibility [5]. According to adjoint manual a value of 1 or less is reasonable.

3.3.3 Flow rate courant scaling

The flow rate courant scaling takes values larger than zero and the default is one. The smaller the value, the less aggressive is the algorithm implied, that encourages the stability of AMG solver [2].

3.3.4 Under relaxation factor

The under-relaxation factors (URF) of Adjoint Momentum, Adjoint Pressure and Adjoint Local Flow Rate could be adjusted as well, obtaining values between 0 and 1. Higher value indicates to higher contribution of new solution to old one which might lead to solver instabilities. The default value was set for all URF to 0.6.

3.3.5 Algebraic multigrid

The tolerance of convergence as well as the Maximum Iterations for inner Algebraic Multi Grid (AMG) iterations can be edited under this function.

3.4 Stabilized Scheme

The ANSYS Adjoint solver includes two stabilization schemes which are capable to handle instabilities of adjoint solution mainly in large cell counts and complex geometries. The Modal as the spatial stabilization scheme is based on the identification of unstable growth patterns in the adjoint solution. There are some available settings that could be adjusted by a user, aiming to a converged solution.

3.4.1 Modal Stabilization Scheme

The Modal Stabilization Scheme implementation relies on two levels instability identification. The first level of instability detection operates as a lightweight monitoring to screen any unstable pattern. In that level, the adjoint solution is manipulated by the primary advancement algorithm. In case this algorithm fail to correct the adjoint solution, is applied a more intensive procedure. A fixed point iteration scheme is used to handle the instable patterns. The Modal settings are illustrated on Figure 4.16
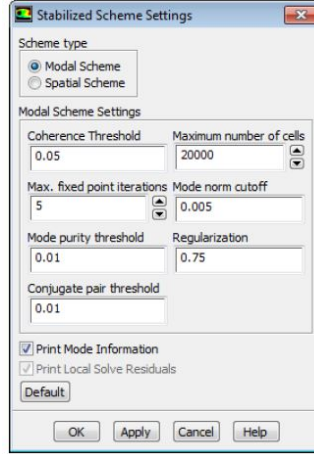
Figure 3.3: *Modal stabilized scheme settings.*

- **Coherence Threshold** defines the threshold for relative variance of growth between iterations at which a more detailed search is activated. Setting smaller values is delayed the activation of more detailed search foe unstable growth [2].

- **Max fixed point iterations** controls the maximum number of iterations required to handle the unstable pattern during the deeper search [2].

- **Mode purity threshold** describes the tolerance for an acceptable unstable pattern. Reducing this value will lead to more detailed search of a more pure unstable mode, yet it increases the cost of simulation, time wise [2].

- **Conjugate pair threshold** is the threshold of a second unstable mode alongside a candidate mode, forming a conjugate pair. That refers to a pseudo-time-periodic instability, versus purely exponential growth. Increasing this value will increase the occurrence of a second mode being included [2].

- **Maximum number off cells** defines the maximum number of cells of an unstable pattern that will be handled it by the modal stabilization scheme [2].

- **Mode norm cut off** applied in order to identify the main body of an unstable pattern and distinguish it from the peripheral spatial of the mode that are small amplitude [2].

- **Regularization** is used to regularize the advancement of the unstable mode components. Its values varies between 0 and 1, where higher value tend to increase the adjoint computational cost [2].

3.4.2 Spatial Stabilization Scheme

The Spatial scheme is applied to handle unstable growth pattern, which have been identified beforehand. The unstable mode and tracking and handling is operated automatically yet some setting could be edited. The ANSYS manual recommends to maintain the default values as they are shown in Figure 3.4

The four settings on the left side on the interface refers to unstable mode tracking and selection, while those on the right are focused on the responce once a mode is identified.

- **Tracking history length** corresponds to the number of iterations that are required during unstable pattern identification. The range of values is set between 2 and 5 where higher the value, better the quality of identification process [2].
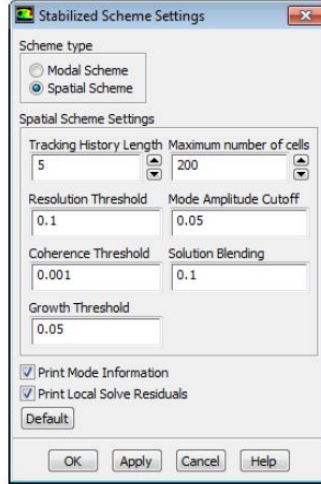
Figure 3.4: *Spatial stabilized scheme settings.*

- **Resolution threshold** refers to a threshold for the separation between modes based on their amplitudes [2].

- **Coherence Threshold** describes a threshold that must be met before an unstable mode is considered as having been identified [2].

- **Growth Threshold** sets the growth rate threshold for unstable modes that must be met before the algorithm get activated. [2].

- **Maximum number off cells** defines the maximum number of cells of an unstable pattern that will be handled it by the spatial stabilization scheme [2].

- **Mode amplitude cut off** define the fraction of the peak mode amplitude beyond which cells will be included for stabilization [2].

- **Solution Blending** represent an URF that blending the stabilized part of the scheme with the standard advancement scheme [2].

3.5   Mesh Morphing

The boundary as well as the interior mesh modification is based on the gradient algorithm which was described in the Chapter 1. The ANSYS morpher is equipped with the so-called Control-Volume Morphing tool (Figure 3.5) and the mesh is edited according to the user's desire.

Firstly, the definition of the modifying zones allows the mesh morphing on specific boundaries. What follows is the definition of the volume mesh where the boundary and the interior mesh are going to be deformed. As soon as these settings are defined, the scale factor for the deformation is chosen. By clicking on Update button, the computation of the control-point sensitivities and the surface deformation takes place. A prediction of the mesh modification to the desired observable is obtained by the Expected Change function. The last step indicates the final mesh modification according to the above settings [2].
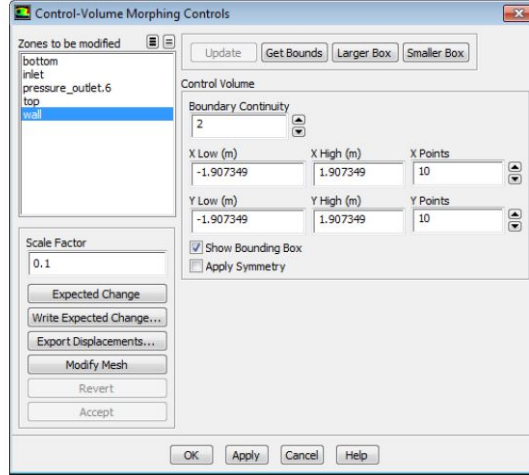
Figure 3.5: *Control-Volume Morphing tool.*

3.6 Given geometries

The front floor duct consists of an inlet and four outlets which guide the air on the drivers pedal area. The geometry as well as the place of the duct are illustrated in Figure 3.6. The rear floor duct includes two ducts with common inlet and four outlets in two pairs. They guide the air to the floor in the back seat Figure 3.7. This duct is symmetrical so only the half duct was simulated. The B-pillar duct has a single inlet and an outlet as boundary conditions and guides air towards back seat passenger. Figure 3.8 shows its position in the vehicle. The last case involved a front ventilation duct system which guides the air towards both the passenger and the driver sides. The system has a common inlet and four different ducts with equal number of outlets (Figure 3.9).
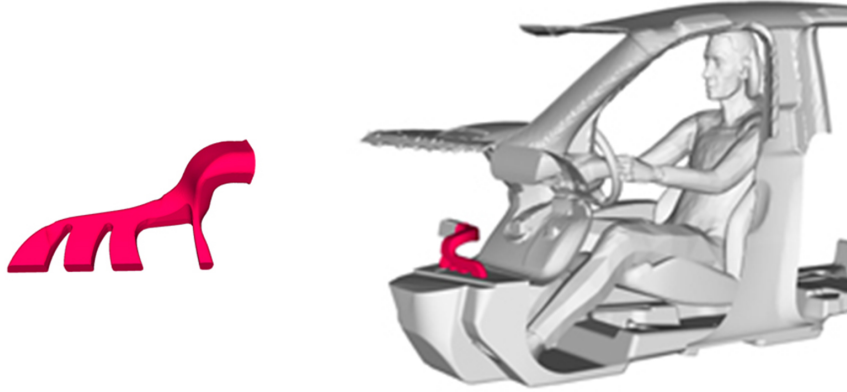
Figure 3.6: *Front floor duct.*
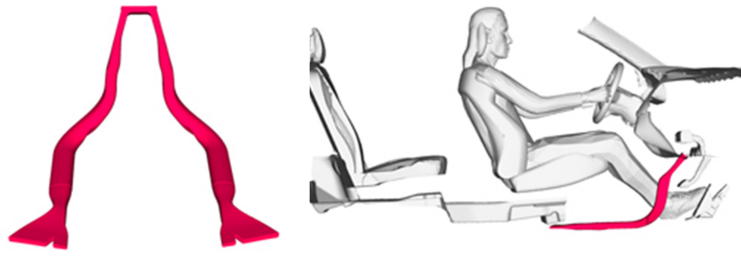
Figure 3.7: *Rear floor duct.*
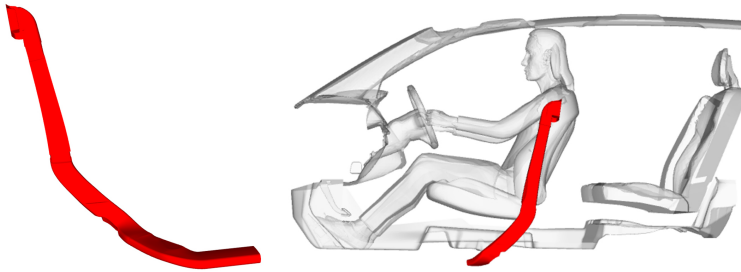
Figure 3.8: *B pillar duct.*
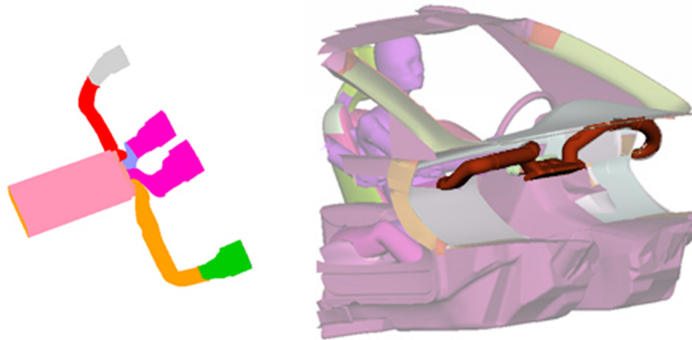
Figure 3.9: *Front ventilation.*

4 Methodology results

Several results were obtained by experiencing the adjoint solver and the ANSYS morphing tool in different geometries. Those results played a decisive role in the methodology establishment. It was investigated how parameters, such as the role of the mesh and the under relaxation factors, could influence adjoint solution. Moreover, factors such as how the complexity of geometry could influence the adjoint stability and morphing tool abilities, were examined.

4.1 Mesh

The mesh is an important factor that could influence the result of both a flow and an adjoint simulation. Both Harpoon and ANSA have been tested, examining their ability to build mesh which will yield to a stable adjoint solution. Harpoon was initially examined due to its extended use on the department.

4.1.1 Harpoon as a mesher

The Harpoon is a quick mesher but it lacks to minimize the amount of skewed cells. According to the Harpoon manual, skewness up to 0.99 can be used in flow cases without influencing the final solution [12].On the other hand, issues may appear in adjoint solver which requires skewness value below 0.8, as ANSYS assistant claimed. In most of the cases, around 0.1% of volume mesh included cells with skewness higher than 0.8. The type of generated mesh was Tetrahedral. A coarse as well as a fine mesh were tested aiming for y+ values higher than 30 or lower than 5 respectively.

Figure 4.1 illustrates the best adjoint convergence which was obtained using the Harpoon. Some parameters such as course mesh,as well as the choice of low order discretization scheme(further explanation in Chapter 4.2) contributed to that solution, yet the bad quality of cells lead to divergence.
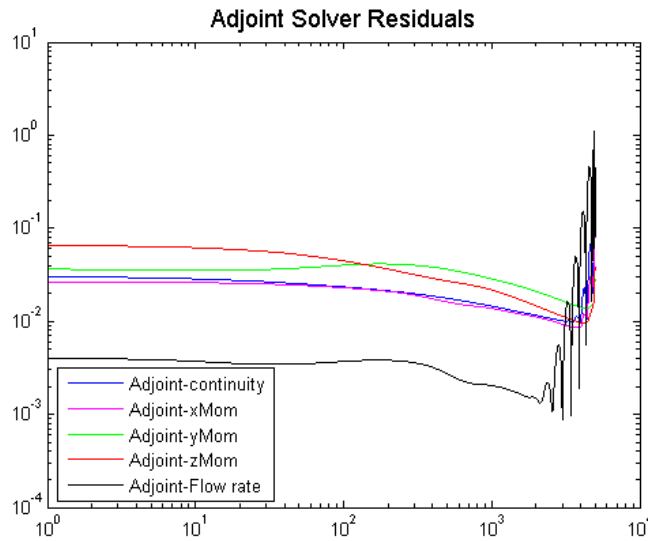

Figure 4.1: *Front floor duct, adjoint residuals using Harpoon.*

Thus, the main issue of Harpoon as a meshing tool was proved to be the difficulty of obtaining cell skewness below 0.8, something that could influence the adjoint solver both in stability and convergence.

4.1.2 ANSA as a mesher

The ANSA software was used as well. Its ability of building better quality mesh than Harpoon is illustrated in Figure 4.2 and Figure 4.3 , where the cell and solid(refers to the volume mesh) skewness is slightly below 0.8. Both a fine and a coarse meshes were generated using ANSA, aiming to obtain adequate cell skewness.
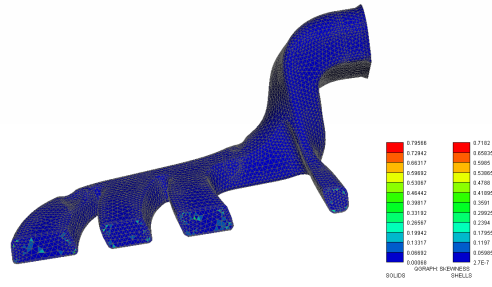
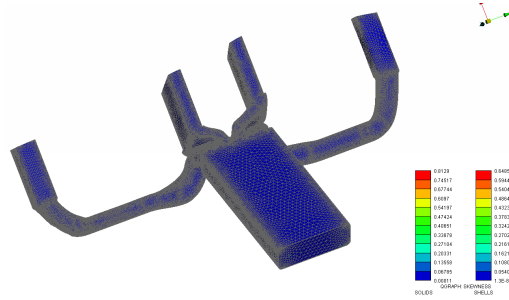Figure 4.2: *Front floor duct, cell skewness using ANSA.*

Figure 4.3: *Front ventilation, cell skewness using ANSA.*

The decent cells quality in combination with only a coarse mesh and low order discretization scheme(Chapter 4.2) resulted in a converged solution as it is shown in Figure 4.4. This makes ANSA a preferred meshing tool for adjoint cases.
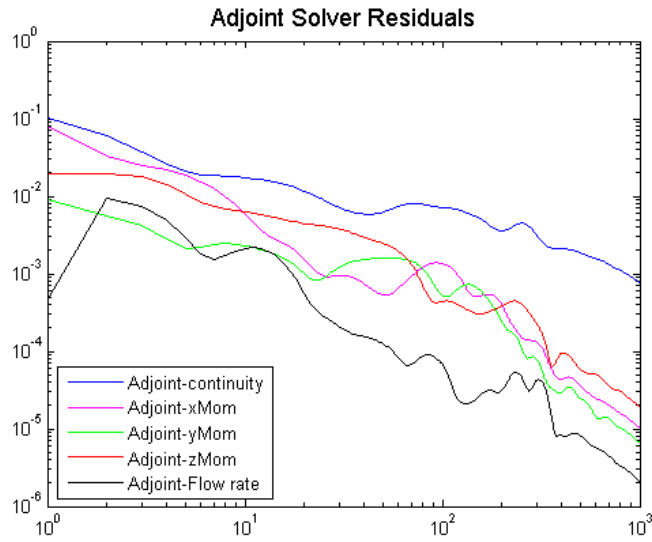

Figure 4.4: *Front floor duct, cell skewness using ANSA.*

4.1.3 Polyhedral mesh

In contrast to the Tetrahedral mesh, the Polyhedral mesh arises better morphing skills. The Tetrahedral meshed cases appeared a high skewness or a negative volume into the domain during the morphing procedure. On the other hand, the Polyhedral mesh properly worked, running more iterations in the adjoint loop. A comparison in the morphing abilities of the Tetrahedral and the Polyhedral mesh is illustrated in Figure 4.5 and Figure 5.10 respectively. The Tetrahedral mesh was modified nine times until the skewness increased, causing adjoint instabilities. In contrast, the Polyhedral mesh morphed twenty eight times showing clearly its morphing advantage.

(a) *1st Adjoint case*   (b) *3rd Adjoint case*

(c) *6th Adjoint case*   (d) *9th Adjoint case*
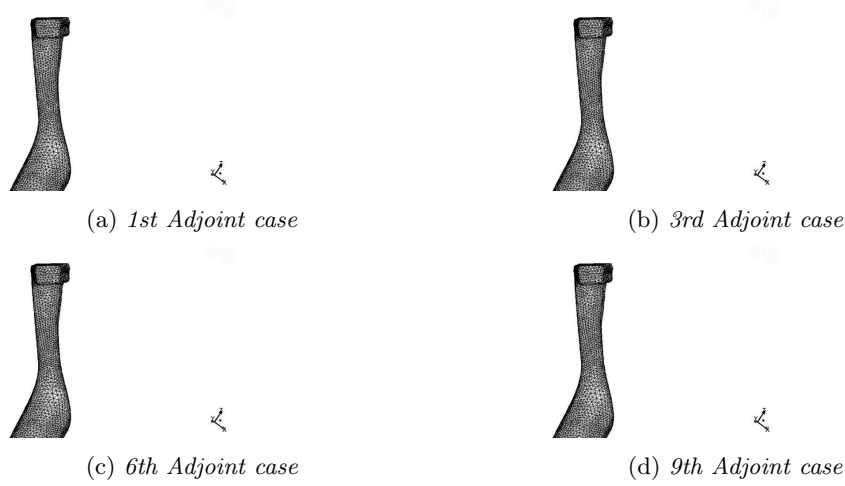
Figure 4.5: *Mesh modifications over adjoint cases, Tetrahedral mesh, rear floor duct.*

(a) *1st Adjoint case*   (b) *9th Adjoint case*

(c) *18th Adjoint case*   (d) *28th Adjoint case*
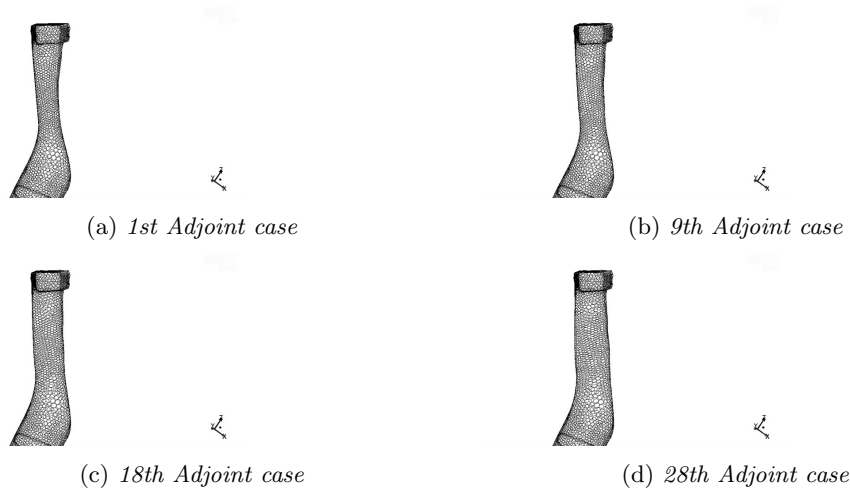
Figure 4.6: *Mesh modifications over adjoint cases, Polyhedral mesh, rear floor duct.*

The adjoint solver converged when tetrahedral or polyhedral coarse mesh was used. Generally, a coarse mesh lacks in solution accuracy in comparison with a fine mesh. According to the CD Adapco technical report, an advantage of polyhedral mesh is the existence of more neighbors cells than in case with tetrahedral mesh [7]. In areas such as long wall edges and at corners, polyhedral mesh seems to have couple of neighbors than tetrahedral. This might yield to better gradient approximation during adjoint simulation, something crucial considering that the course mesh is used for all cases. Moreover, it seems that Polyhedral mesh is less sensitive in stretching than Tetrahedral mesh, maintaining adequate cell skewness for many adjoint cases. Thus, Polyhedral mesh seems to be a proper choice for meshing our geometries.

4.2 Adjoint discretization scheme

The adjoint discretization scheme impacts on the accuracy of the adjoint solution since the higher the scheme order, the lower the numerical error. It was recommended to use the second order upwind scheme for the momentum equation on the adjoint solver. In flow solution the second order upwind scheme provides higher accuracy due to the fact that it minimizes the numerical discretization error (numerical diffusion). The second order upwind scheme achieves more accurate finite difference results for the approximation of spatial derivative including three data points instead of just two as in first order upwind scheme. While the higher order scheme may result in greater accuracy, it can also result in convergence difficulties and instabilities at a certain flow condition since the higher derivatives in the leading truncation terms of Taylor expansion may be large and the overall numerical scheme might be numerically instable.

As it is seen in Figure 4.7 there is a side-by-side comparison of the schemes used for the flow solver and for the adjoint solver. Using the same scheme for the adjoint solution and the flow solution yields the most accurate discrete derivative calculation [2].
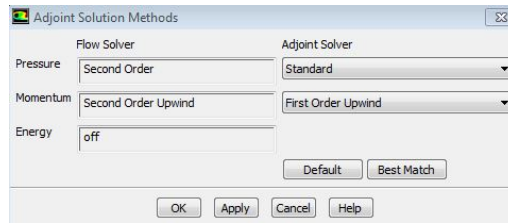
Figure 4.7: *Adjoint solution methods.*

The Best Match option attempts to match the different solvers schemes. This matching is considered to provide more accurate sensitivity calculations. In the case of pressure scheme there was not any matching between flow and adjoint solver so the standard scheme was used. The second order upwind scheme was chosen for the momentum discretization.

The convergence instabilities of second order scheme led us to use the first order scheme, resulting to the desired adjoint converged solution as it is shown in Figure 4.8.
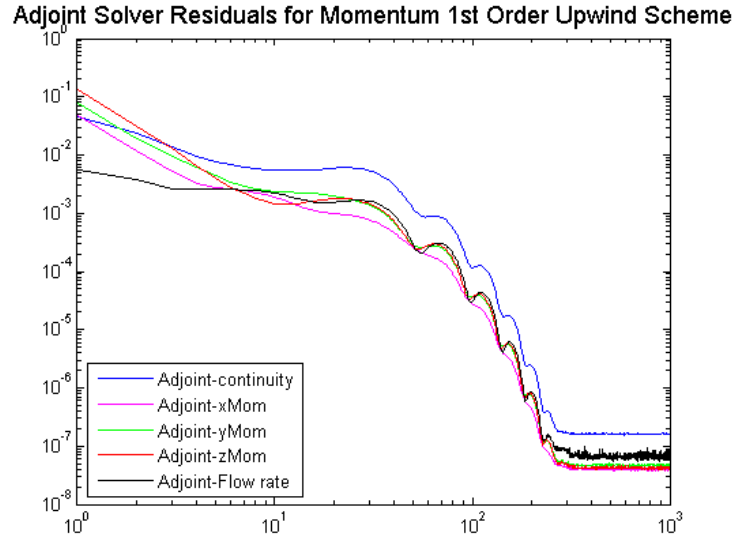

Figure 4.8: *Adjoint Solver Residuals for Momentum 1st Order Upwind Scheme.*

Moreover, the possibility to initialize the domain solution by using the the first order upwind scheme solution and then apply the second order upwind scheme, was investigated. However, the residuals rapidly increased, the stabilization scheme was unable to handle the unstable patterns resulting to a diverged solution (4.9).
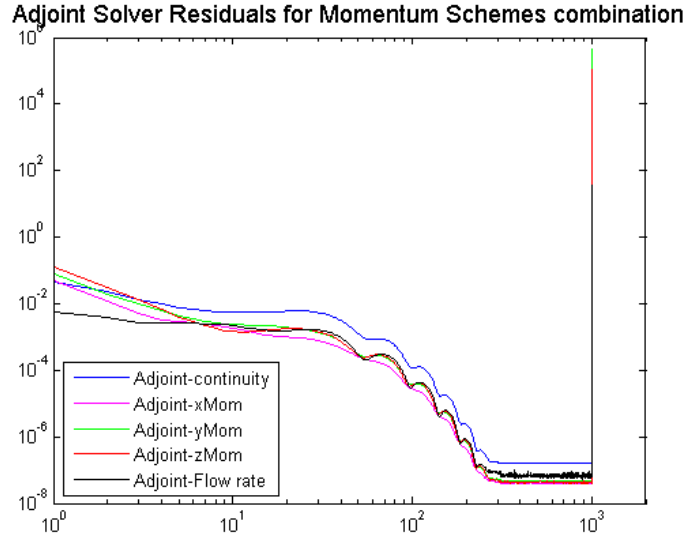
18

Figure 4.9: *Adjoint Solver Residuals for Momentum 1st and 2nd Order Upwind Scheme.*

4.3   Domain partitioning

Different adjoint results were obtained when running cases on the cluster and in the work station. Even if a converged solution was computed in a work station, no convergence could be achieved when using the cluster. Figure 4.10 shows the diverged solution which runs in cluster using 120CPUs. This fact leads to examine the contribution of the mesh partitioning in final solution.
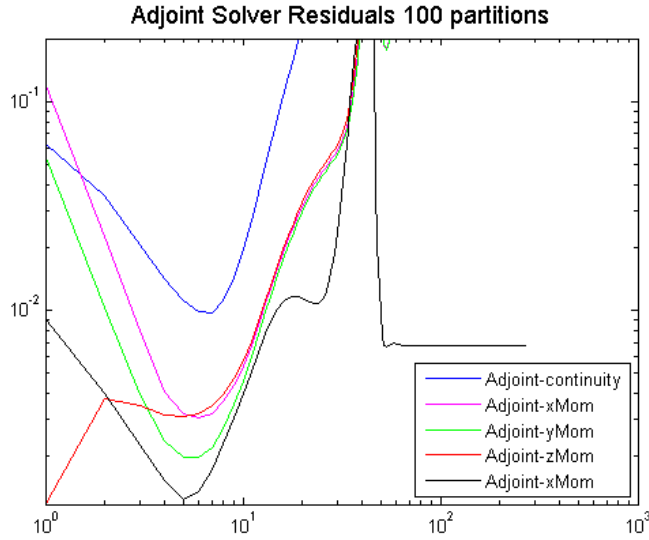

Figure 4.10: *Adjoint Solver Residuals for rear floor duct.*

On the following Figure 4.11 and Figure 4.12 two different partitioning setups for exactly the same case are illustrated.

Several combinations of partitioning and CPU number were operated resulting in the reduction of CPU number to 8, using 16 mesh partitions. That combination lead to converged adjoint solution and the residuals are illustrated in Figure 4.13.
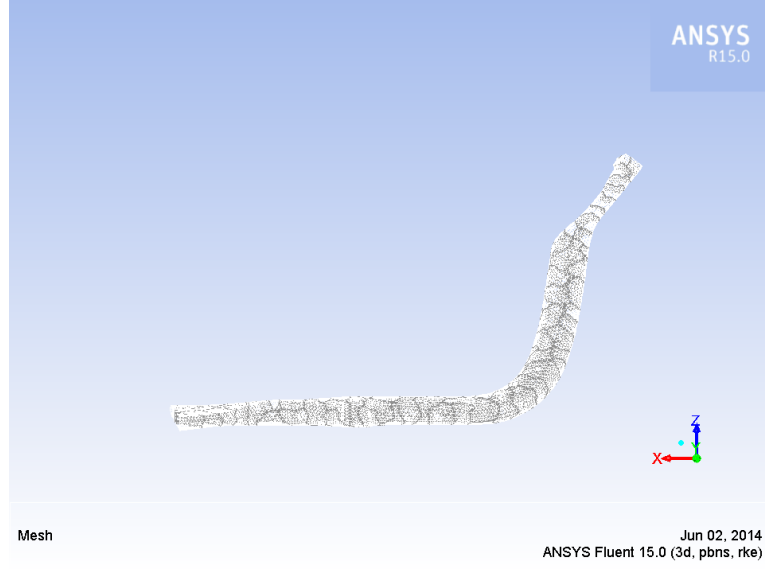
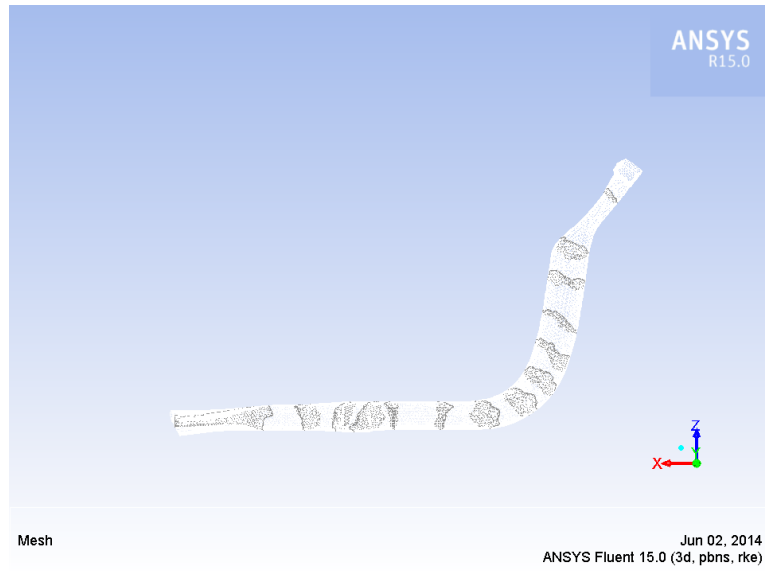Figure 4.11: *100 mesh partitions for front floor duct.*

Figure 4.12: *16 mesh partitions for front floor duct.*

When working with higher number of mesh partitioning and CPUs, modal stabilization scheme seems to have a lack in efficient communication between its sub-iterations, resulting in difficulties in handling the unstable patterns. A hypothesis might be that the number of partitions effect the number of required halo cells which are essential for communication between different mesh partitions [10]. The same method takes place in flow simulation splitting the domain in smaller parts and compiling the results at the end. In contrast with flow simulations, adjoint solver seems to be sensitive to partitioning.

It is worth mentioning that using 8 CPUs and 100 mesh partitions, the adjoint diverged. Consequently, both the number of CPUs and partitions should be maintained low.
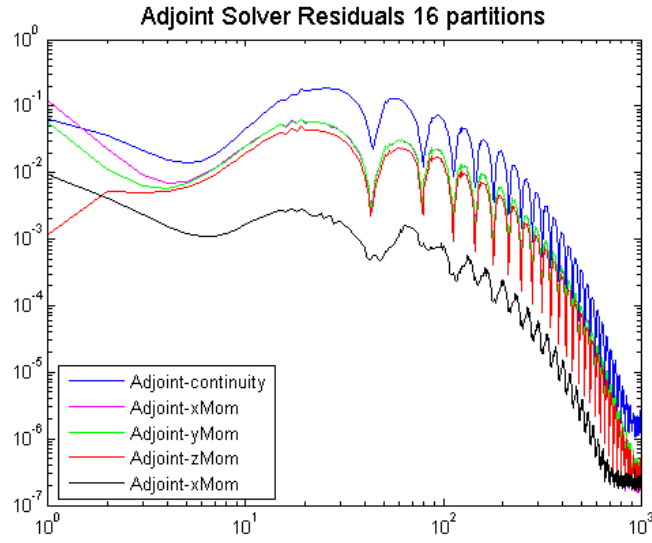
Figure 4.13: *Adjoint Solver Residuals 16 partitions, rear floor duct.*

4.4 Domain Morphing

The ANSYS Control Volume Morphing tool is used to modify both the surface and the interior mesh with respect to the cost function. Chapter 1 and Chapter 2 described a more detailed description about its algorithm and its parameters. When experiencing that tool, it was found that it is sensitive on grid parameters (Chapter 2.6), yielding skewed cells or negative volume, disturbing any further adjoint investigation. Therefore, the choice of proper values for grid became a necessity. In Figure 4.14 the interface of the morphing tool and the rectangular volume that defines the future modified areas, are illustrated.
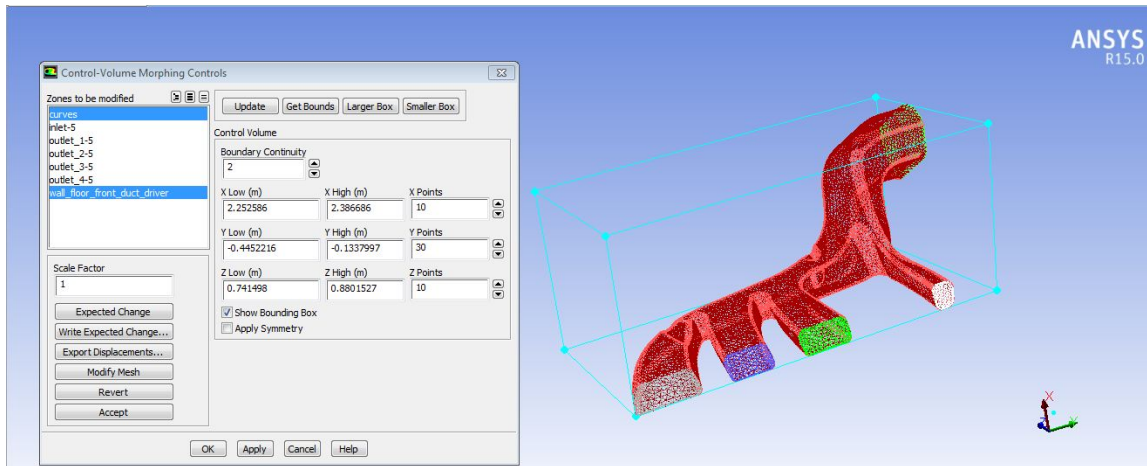
Figure 4.14: *Mesh morphing interface, front floor duct.*

In the tool interface, the rectangular volume coordinates appear, described as X Low (m) and X High (m) for x coordinates. Also, the number of control points are defined under the X Points for the relative coordinates. As it was described in Theory Chapter and in Equation 2.23, the modification movement is applied on control points resulting in smooth repositioning of the grid nodes. This is achieved through the following

equation,

$$\alpha = \frac{X_{high} - X_{low}}{X_{point}} = \frac{Y_{high} - Y_{low}}{Y_{point}} = \frac{Z_{high} - Z_{low}}{Z_{point}} \tag{4.1}$$

keeping constant the derived value of α it is easy to calculate the number of Y Points and Z Points. In that way, a smooth deformation will be applied in the whole domain reducing the chance of negative volume appearance.

4.5 Stabilization scheme

Usually, the adjoint solution follows a standard pattern. During the initial iteration, the adjoint shows a convergence trend ,then instabilities appear due to the growth of the unstable pattern. The stabilization scheme is applied aiming to absorb the instabilities and the adjoint oscillations. That procedure is repeated over the defined number of adjoint iterations leading to a converged solution at the end.

Modal Stabilization Scheme was used in most of the cases due to its ability to absorb better the high adjoint fluctuations than Spatial Scheme. A comparison between those schemes is illustrated in Figure 4.15 and Figure 4.16.
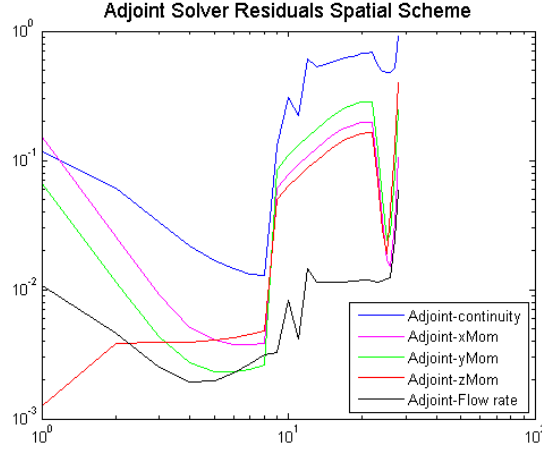

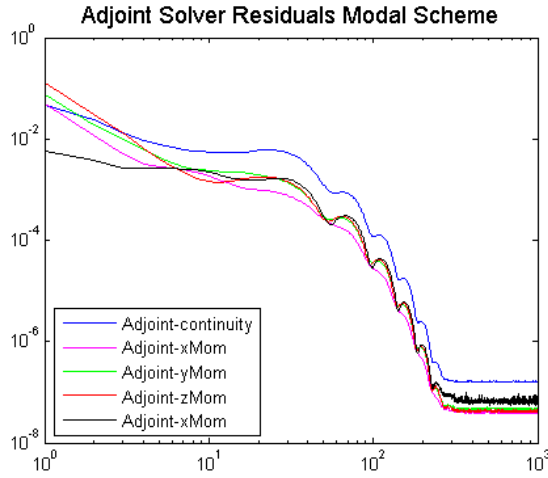Figure 4.15: *Spatial stabilization scheme, front floor duct.*

Figure 4.16: *Modall stabilization scheme, front floor duct.*

The Coherence Threshold, the maximum number of cells and the Regularization could be considered as the most effective editable parameters in a modal scheme. The proper values for these settings were obtained ,monitoring the log file of the adjoint simulation. An example of the log file is illustrated on Figure 4.17


```
Mode growth:     1.12889e+00  Coherence:     2.00725e-02
Growing pattern cell count: 21116
Too many cells in growing pattern (21116) - delaying search
```

Figure 4.17: *Log file.*

The outcome of Figure 4.17 is the identification of unstable grown pattern. The mode growth factor describes that an unstable pattern grows by more than 12% in one iteration. Also, the number of cells that are involved in that pattern is 21116. Therefore, through the Coherence Threshold and the maximum number of cells options, modal stabilization could be triggered and handle adjoint solver fluctuations.

4.6 Under relaxation factor

During the current study the contribution of the under relaxation factors of the Adjoint Momentum and the Adjoint Continuity in the adjoint convergence was investigated. The default value of the Adjoint Momentum and the Adjoint Continuity URF is 0.6. As it is seen in Figure 4.18 many solution oscillations appeared which could not be handled by the stabilization scheme and solution diverges in seventy iterations.
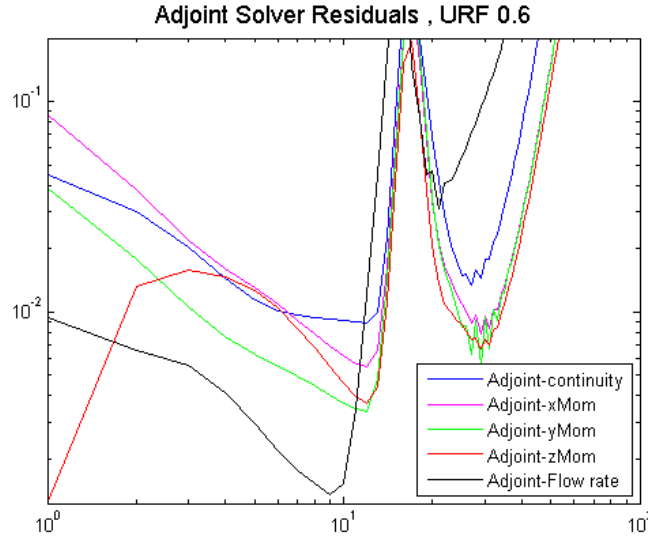

Figure 4.18: *Adjoint Solver Residuals URF 0.6.*

In contrast, including smaller percentage added in the new solution, stabilization scheme could handle the instabilities and show a better convergence trend as it is shown on Figure 4.19.

When trying to reduce more the URF , the residuals behaved better, appearing small solution fluctuations. Yet, the solution was not converged exhibiting a neutral trend.
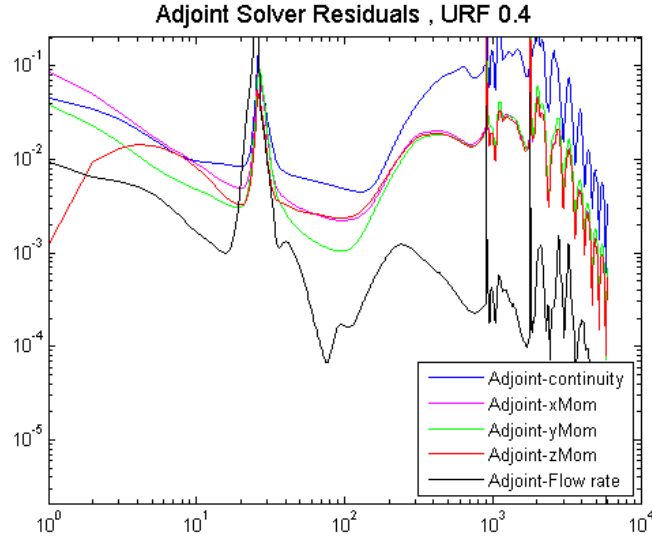
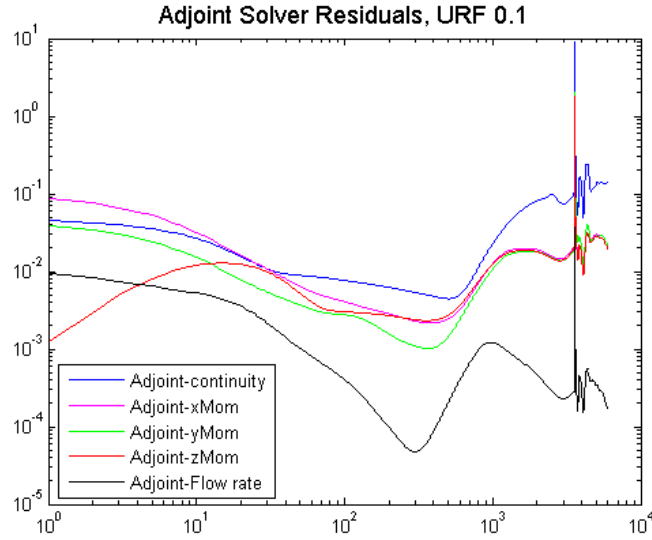Figure 4.19: *Adjoint Solver Residuals URF 0.4.*

Figure 4.20: *Adjoint Solver Residuals URF 0.1.*

As it is seen through the previous Figures, the under relaxation factor can influence the solution ,yet it can not lead to a converged solution by itself, so, other factors need to be considered as well.

4.7   Boundary modifications

In most simulations at VCC, extensions are made on the inlet and the outlet boundary conditions. Mainly, aiming to have a fully developed flow that enters and exits the duct. It is a general condition that should be fulfilled in any CFD simulation in order to obtain adequate results. Figure 4.21 illustrates the common outlet box that is used in most of the climate simulations.

The sharp edges on the contacting points between the duct nozzle and the outlet box lead to flow separations and consequently to high pressure gradients. The adjoint solver seems to lack in computing properly the sensitivity field on the surfaces around the flow separation areas, resulting in computational instabilities. Thus, in the adjoint cases modifications on the outlet boxes were required.
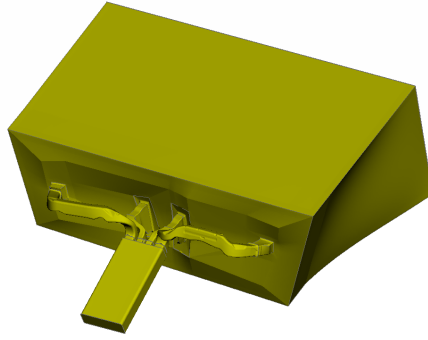
Figure 4.21: *B-pillar duct,outlet box.*

Figure 4.22 illustrates the modified outlet boxes. The lack of separations regions around the outlet seems to effect adjoint stability.
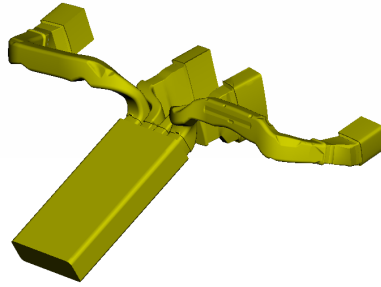

Figure 4.22: *B-pillar duct,separated outlet box.*

Further simplifications were required for adjoint convergence, such as the guide vanes into the ducts were removed. Moreover the coarse mesh could not represent smoothly the fins or any other detailed geometry. When these simplifications were made, the adjoint residuals showed a better trend. The simplified case is illustrated in Figure 4.23.

Figure 4.23: *B-pillar duct, nozzle without fins.*

5 Adjoint results

This Chapter undertakes the outcome of the adjoint solver. Morphed meshes as well as the flow results of some geometries will be presented. The methodology findings ruled the adjoint simulations as they were presented in the previous chapter.

5.1 Contour of normal optimal displacement

The mesh displacement analysis was operated through the contour of normal optimal displacement. Figure 5.1 and Figure 5.2 show the contour of normal optimal displacement of front floor duct. Red illustrates a deformation inwards and blue outwards of volume mesh.
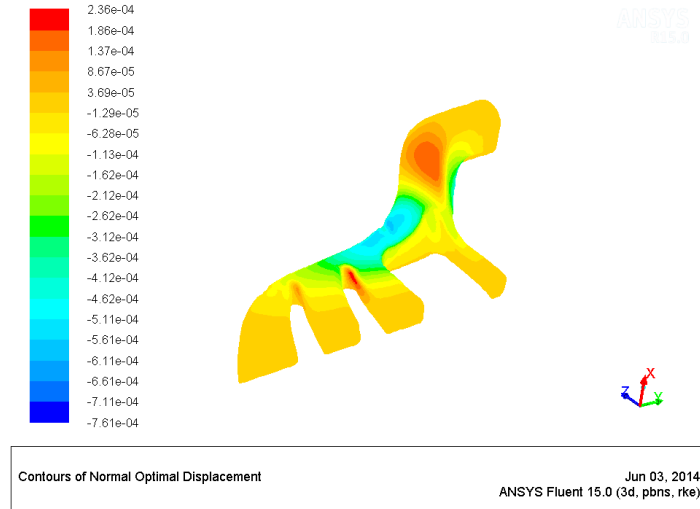
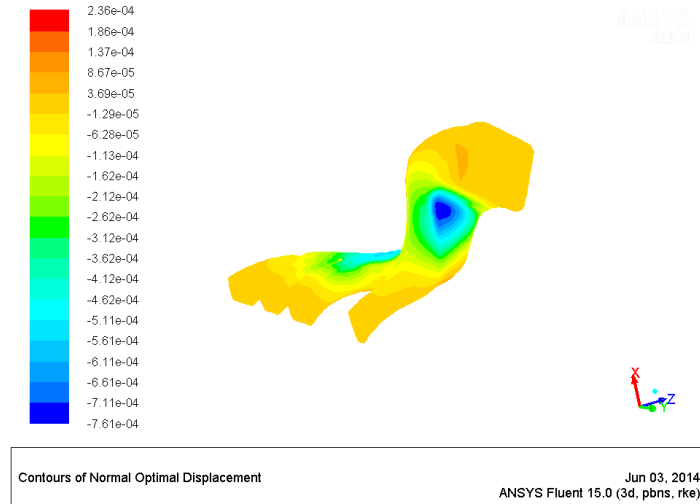Figure 5.1: *Contour of optimal displacement, front floor duct.*

Figure 5.2: *Contour of optimal displacement, front floor duct.*

It is worth mentioning that the sensitivity field has been computed for whole domain since morphing tool was applied without any topology limitations. Figure 5.1 and Figure 5.2 illustrates the potential displacement

of the mesh after the first adjoint iteration. The sensitivity field will iteratively change when running the loop. The contour of normal optimal displacement after thirteen iterations is shown in Figure 5.3.
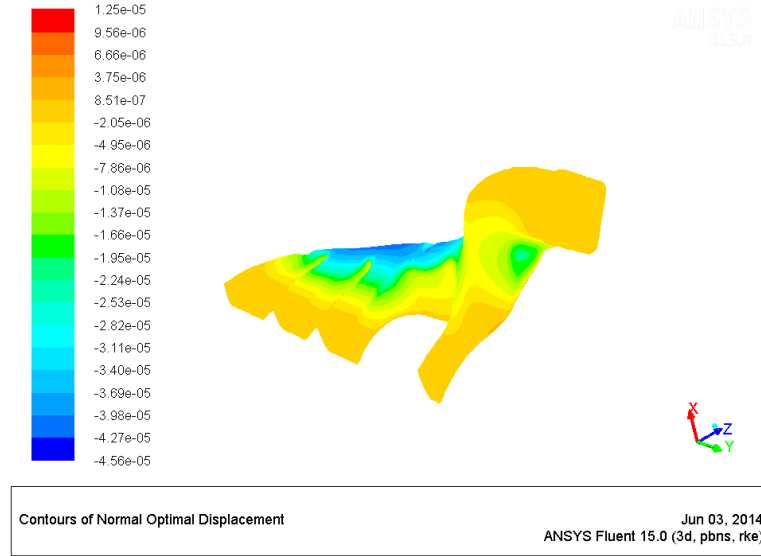

Figure 5.3: *Contour of optimal displacement in 13th adjoint loop, front floor duct.*

In real engineering problems, the mesh deformation is limited by the duct surrounding. Having examined the surrounding, the non-deformed areas could be identified. In Figure 5.4 two of the front ventilation ducts are seen, green represents the regions where deformation is allowed and red shows the locked areas.
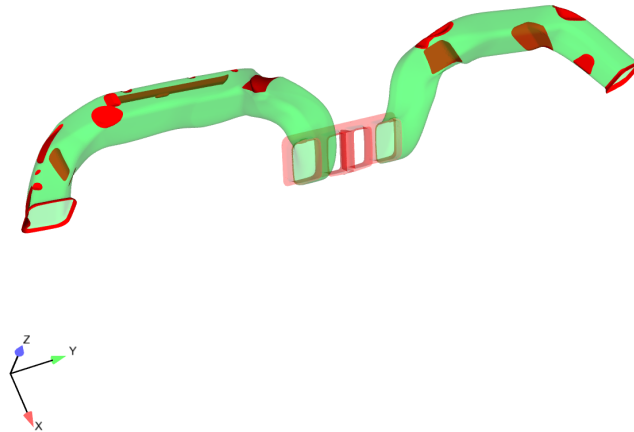

Figure 5.4: *Front ventilation deformation regions.green and red shows the free and locked areas respectively.*

These restrictions influence the contour of normal optimal displacement. For example, in Figure 5.5 the contour of normal optimal displacement of the driver side duct without considering any constraints is seen. The contour is different when some of the regions are locked as is depicted on Figure 5.6. Furthermore, the existence of many locked areas leads to less mesh modifications and consequently in less pressure drop decrease.

Thus, the surrounding of a duct should be carefully examined in order for the mesh constraints to be set.
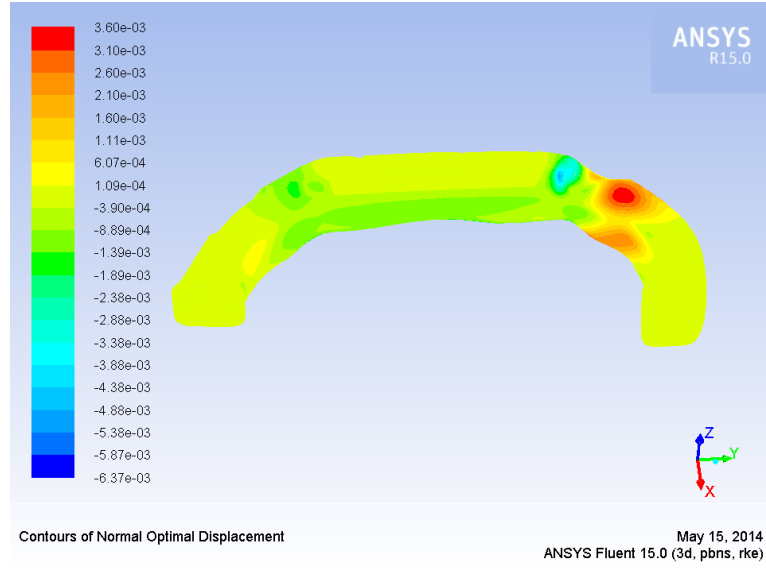

Figure 5.5: *Contour of normal optimal displacement without constraints, front ventilation.*
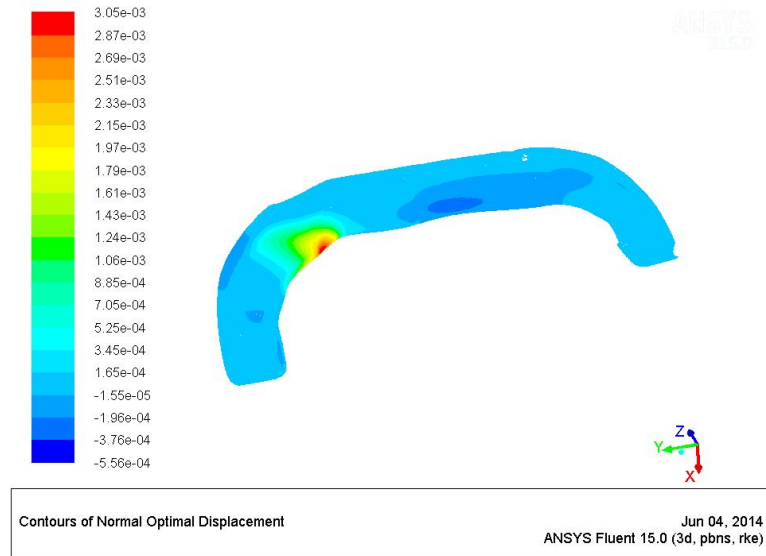

Figure 5.6: *Contour of normal optimal displacement with constraints, front ventilation.*

5.2 Pressure drop

The cost function in the current thesis is pressure drop minimization. The decrease of pressure drop depends on the defined geometry constraints as they were explained in the Chapter 5.1. When operating a free deformation on a geometry, a great pressure drop percentage could be achieved. For example, when morphing the front floor duct without considering any topology limitations, the pressure drop could be decreased up to 60% as it is seen on Figure 5.7.
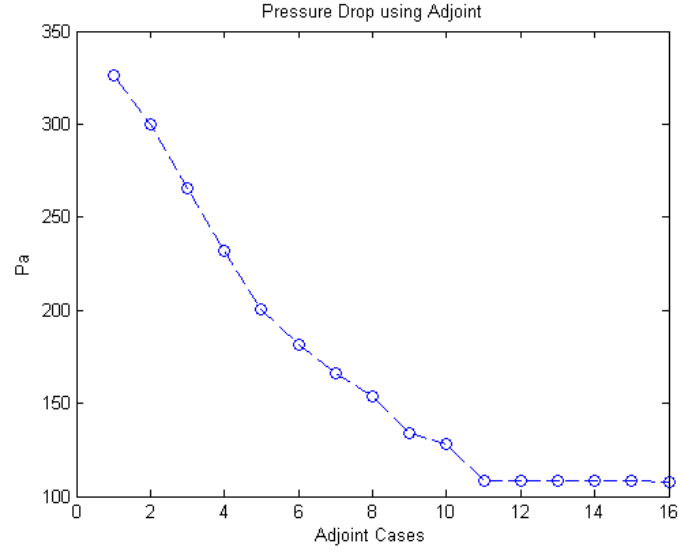
Figure 5.7: *Pressure drop per adjoint case,front floor duct.*

When morphing constraints are present, the minimization of the cost function is bounded by them. The constraints decrease the available morphing room, hence smaller deformations are applied resulting in less pressure drop reduction. For instance, the driver side duct in front ventilation geometry has significantly expanded , reducing the total pressure drop by 11% which is illustrated in Figure5.8. However, the 23rd adjoint case has reached the limits of the available space.
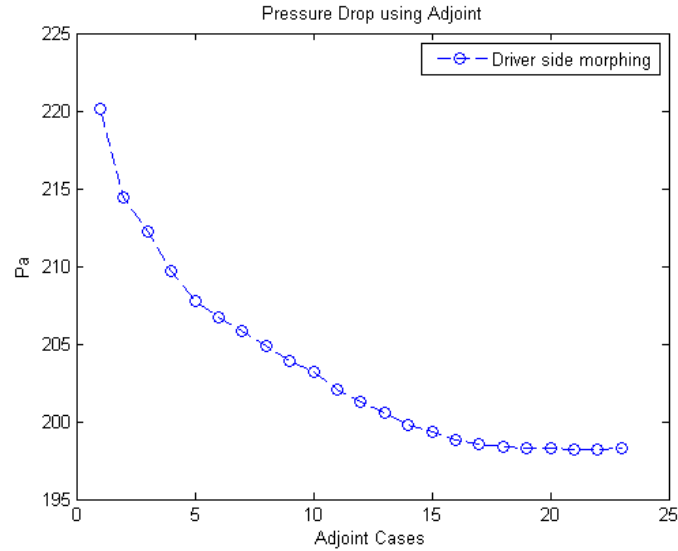

Figure 5.8: *Pressure drop per adjoint case,front ventilation.*

Out of the 23 adjoint cases for the driver side duct, the mesh from the 9th adjoint case reached the limit of available space, so it was used as the base case from which the passenger side morphing began. The front ventilation total pressure drop minimization is illustrated in Figure 5.9.
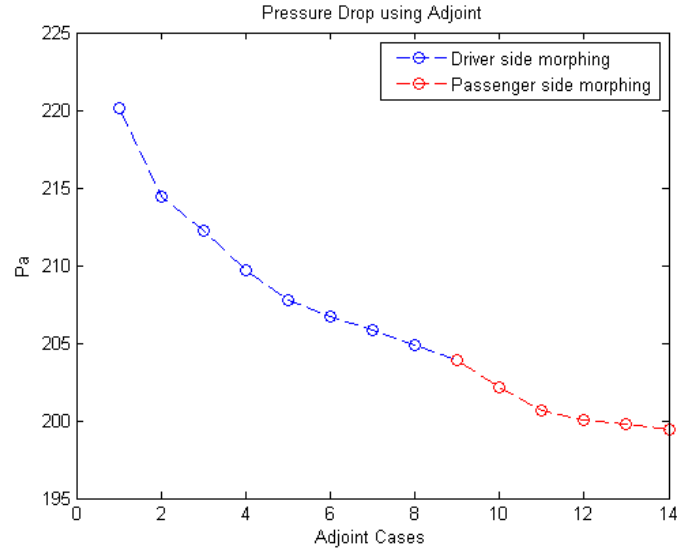
Figure 5.9: *Pressure drop per adjoint case,front ventilation.*

5.3 Flow visualization

Moreover a flow visualization helps to understand the consequences of adjoint solver in the pressure drop reduction. The adjoint solver identifies the separation regions as well as the areas with high velocity gradients and applies changes on them such as a duct's diameter increase or smoothing steep geometry's angles. Figure 5.10a and Figure 5.10b illustrates changes on the rear floor duct, comparing the initial and the final case respectively.
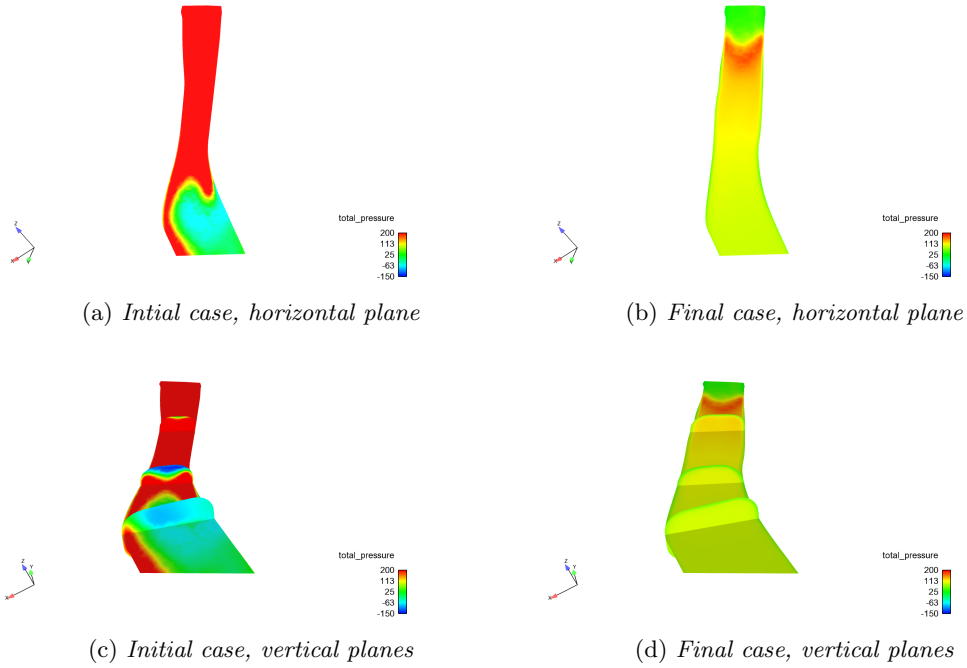

(a) *Intial case, horizontal plane*

(b) *Final case, horizontal plane*

(c) *Initial case, vertical planes*

(d) *Final case, vertical planes*

Figure 5.10: *Mesh modifications over adjoint cases,front floor duct front view.*

The expansion of the most narrow part and the final cylindrical shape of the duct eliminated the separation

regions. Thus, a smooth pressure distribution across the domain was obtained, which resulted into the desired pressure drop minimization. Those changes are clearly seen in Figure5.10c and Figure5.10d.

Equivalent mesh modifications were performed on the B-pillar duct. The morphing area was focused on the middle of the duct, maintaining constant the rest of the geometry. Figure 5.11 and Figure 5.12 illustrate the initial and final geometry respectively. The streamlines and the plotted total pressure on them show the reduction in total pressure across the domain.
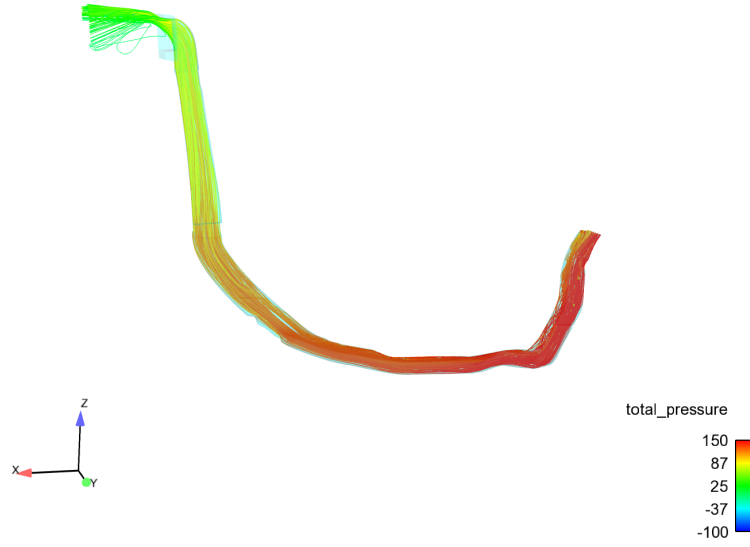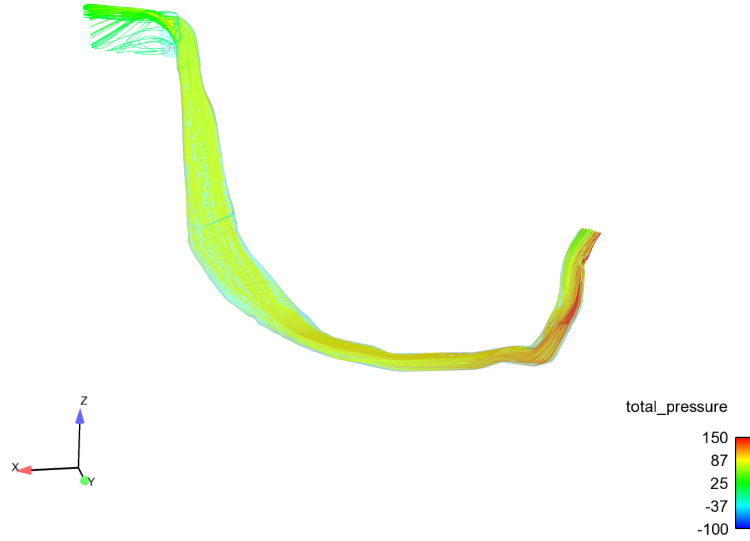

Figure 5.11: *Initial case, B-pillar duct.*

Figure 5.12: *Final case, B-pillar duct.*

6 Discussion

The adjoint solver is a powerful tool which can significantly reduce the development time of a duct. An optimized geometry could be obtained through adjoint procedure in a few days in contrast with the ordinary procedure that requires some weeks.

The cost function in the current thesis is the minimization of the pressure drop which was successfully achieved in all the given geometries. The adjoint procedure properly worked when using coarse polyhedral mesh and the skewness value was below 0.8. Moreover, it was necessary to use low order discretization scheme, the first order upwind due to the fact that higher order scheme was instable leading the solver to diverge. The coarse mesh as well as first order upwind scheme might yield a inaccurate flow and adjoint solution. Thus, the evaluation step in the adjoint procedure, as it was described in Chapter 3, was introduced. When comparing the actual flow results of the fine and the coarse mesh there was a difference between them. In contrast, the percentage of the pressure drop reduction was equivalent. Therefore, the adjoint predicted the right changes which resulted in the minimization of the cost function.

The bottle neck of the adjoint procedure is the morphing tool which is not mature enough to cover a wide application range. The morphing function of ANSYS didn't seem to be able to handle a system of ducts at the same time. Moreover, the existence of skewed cells (a value higher than 0.8) and the generation of negative volumes into the domain, restricted the adjoint procedure.Thus, the introduction of a new step into the adjoint loop is required in order to overcome the morphing issues.

To summarize, the required settings for the adjoint procedure are shown on Table 6.1

Mesh type	Polyhedral
Mesh density	Coarse
Cell skewness	~0.8
Momentum discretization scheme for adjoint solver	First order upwind
Mesh morphing	Constant a

Table 6.1: Basic settings for adjoint solver.

7 Future work

The adjoint loop which was followed in the current thesis is illustrated in Figure 7.1. The loop is sensitive to volume morphing where skewed cells or negative volume appear after several loop iterations.
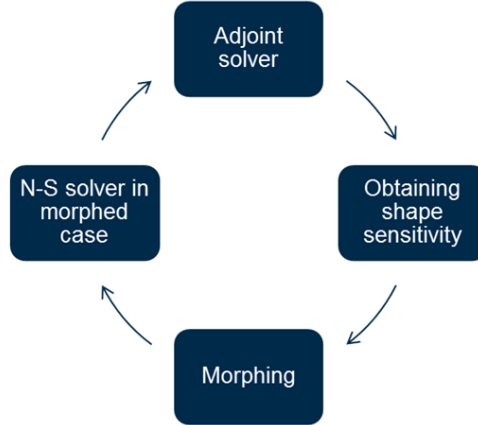

Figure 7.1: *Adjoint loop,current thesis.*

The replacement of the volume morphing step and the introduction of two new steps in the adjoint loop could overcome this issue. The surface sensitivity will be followed by surface morphing and regeneration of the volume mesh, instead of morphing the volume. Thus, the volume mesh will have adequate cell skewness in any single iteration of the adjoint loop. The suggested procedure is shown on Figure 7.2.
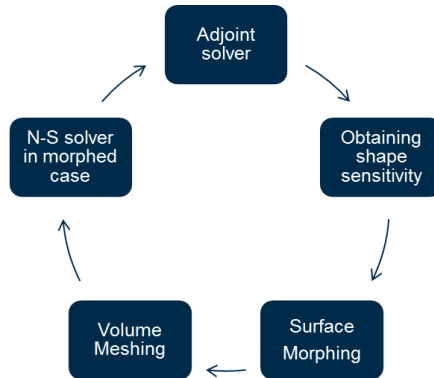

Figure 7.2: *Adjoint loop,suggestion.*

References

[1] J. J. Alonso. A Crash-Course on the Adjoint Method for Aerodynamic Shape Optimization (2003).

[2] *ANSYS FLUENT Manual. ANSYS FLUENT Adjoint Solver*. Version 14.5. ANSYS, Inc., 2012.

[3] N. Bakhvalov. Courant–Friedrichs–Lewy Condition. *Encyclopedia of Mathematics* (2001).

[4] A. C. Duffy. *An introduction to gradient computation by the discrete adjoint method*. Tech. rep. Technical report, Florida State University, 2009.

[5] J. H. Ferziger and M. Perić. *Computational methods for fluid dynamics*. Vol. 3. Springer Berlin, 1996.

[6] T. Han et al. Adjoint Method for Aerodynamic Shape Improvement. *Training* **2006** (), 06–28.

[7] M. Peric and S. Ferguson. *The advantage of polyhedral meshes*. Tech. rep. Technical report, CD Adapco Group, 2005. www. cd-adapco. com/news/24/TetsvPoly. htm, 2012.

[8] O Pironneau. *Optimal shape design for elliptic systems. 1984*.

[9] J. Reuther et al. *Aerodynamic shape optimization of complex aircraft configurations via an adjoint formulation*. Research Institute for Advanced Computer Science, NASA Ames Research Center, 1996.

[10] Z. Shang. Performance analysis of large scale parallel CFD computing based on Code_Saturne. *Computer Physics Communications* **184**.2 (2013), 381–386.

[11] D. Thévenin and G. Janiga. and Computational Fluid Dynamics (2008).

[12] *User guide*. Version 4.3. HARPOON.